







Coexisting magnetic structures and spin reorientation in $\text{Er}_{0.5}\text{Dy}_{0.5}\text{FeO}_3$: Bulk magnetization, neutron scattering, specific heat, and density functional theory studies

Sarita Rajput ¹, Padmanabhan Balasubramanian ², Ankita Singh ¹, Françoise Damay,³ C. M. N. Kumar ^{4,5}, W. Tabis ⁵, T. Maitra,¹ and V. K. Malik ^{1,*}

¹Department of Physics, Indian Institute of Technology Roorkee, Roorkee 247 667, India

²Department of Physics, Graphic Era University, Dehradun, Uttarakhand 248 002, India

³Laboratoire Léon Brillouin, CEA-CNRS, CEA/Saclay, 91191 Gif-sur-Yvette, France

⁴Institute of Solid State Physics, Vienna University of Technology, Wiedner Hauptstrasse 8-10, 1040 Vienna, Austria

⁵AGH University of Science and Technology, Faculty of Physics and Applied Computer Science, 30-059 Kraków, Poland



(Received 3 October 2021; revised 12 April 2022; accepted 1 June 2022; published 28 June 2022)

The complex magnetic structures, spin reorientation, and associated exchange interactions have been investigated in $\text{Er}_{0.5}\text{Dy}_{0.5}\text{FeO}_3$ using bulk magnetization, neutron diffraction, specific heat measurements, and density functional theory calculations. The Fe^{3+} spins order as G-type antiferromagnet structure depicted by $\Gamma_4(G_x, A_y, F_z)$ irreducible representation below 700 K, similar to its end compounds. The bulk magnetization data indicate occurrence of the spin-reorientation and rare-earth magnetic moments' polarization below ~ 75 K and 10 K, respectively. The neutron diffraction studies confirm an “incomplete” $\Gamma_4 \rightarrow \Gamma_2(F_x, C_y, G_z)$ spin-reorientation initiated ≤ 75 K. Although the relative volume fraction of the two magnetic structures varies with decreasing temperature, both coexist even at 1.5 K. Below 10 K, the polarization of $\text{Er}^{3+}/\text{Dy}^{3+}$ moments in a c_y^R arrangement develops, which gradually increases with decreasing temperature. At 2 K, magnetic structure associated with c_z^R arrangement of $\text{Er}^{3+}/\text{Dy}^{3+}$ moments also appears. At 1.5 K, while the rare-earth magnetic moments show a $c_y^R + c_z^R$ -type arrangement, the Fe^{3+} spins are represented by a combination of a $\Gamma_2 + \Gamma_4(G_z, G_x)$ arrangement. A clear signature of the magnetic structure with $\Gamma_1(G_y)$ representation, symmetrically compatible with the c_z^R -type arrangement of rare-earth moments, is not confirmed from the refinement of the neutron diffraction data. The observed Schottky anomaly at 2.5 K suggests that the “rare-earth ordering” is induced by polarization due to Fe^{3+} spins. The $\text{Er}^{3+}\text{-Fe}^{3+}$ and $\text{Er}^{3+}\text{-Dy}^{3+}$ exchange interactions, obtained from first principle calculations, indicate that these interactions primarily cause the complicated spin reorientation and c_y^R rare-earth ordering in the system, respectively, while the dipolar interactions between rare-earth moments result in the c_z^R type rare-earth ordering at 2 K.

DOI: [10.1103/PhysRevB.105.214436](https://doi.org/10.1103/PhysRevB.105.214436)

I. INTRODUCTION

Rare-earth orthoferrite materials $R\text{FeO}_3$ (R = rare-earth ion) have shown potential for technologically relevant applications via observation of spin switching, spontaneous exchange bias, and optically controlled ultrafast spin dynamics [1–7]. Additional important properties include the large linear magneto-dielectric effect, spontaneous ferroelectric polarization, multiferroicity, and the magneto-caloric effect [8–13].

The orthoferrite materials belong to the family of perovskites and crystallize in the structure represented by orthorhombic space group $D_{16}^{2h}\cdot Pbnm$ symmetry, as observed in the case of manganite and cobaltate materials [14,15]. Unlike manganites, a long-range static Jahn-Teller effect is absent in orthoferrites [14]. The FeO_6 octahedra in rare-earth orthoferrites possess a GdFeO_3 -type distortion with nearly equal Fe-O bond lengths [16–20]. The structural distortion increases with atomic number of R [21].

The rare-earth orthoferrites ($R\text{FeO}_3$) are antiferromagnets with a Néel temperature (T_{N1}) in the temperature range of 650–760 K [22,23]. An increase in the atomic number of R results in systematic reduction of T_{N1} [23]. At T_{N1} , the orthoferrites undergo transition from a paramagnetic to G-type antiferromagnetic state with ordering wave vector $\vec{k} = (0, 0, 0)$. The magnetic structure belongs to Γ_4 irreducible representation, which can be written as (G_x, A_y, F_z) in Bertaut notation [24]. The Fe^{3+} spins order primarily in an antiferromagnetic G-type configuration along the crystallographic a axis (G_x), while A_y and F_z correspond to the A-type antiferromagnetic and ferromagnetic arrangement of the spins along the crystallographic b and c axes due to covert and overt canting, respectively [23,25,26].

The dominant interaction in all the orthoferrite compounds is an isotropic $\text{Fe}^{3+}\text{-Fe}^{3+}$ superexchange interaction, which is denoted as $J_{\text{Fe-Fe}}$. The additional isotropic interactions are the $R^{3+} - \text{Fe}^{3+}$ and $R^{3+} - R^{3+}$ interactions [25]. The strength of the isotropic interactions is in the following order: $J_{\text{Fe-Fe}} > J_{R\text{-Fe}} > J_{R\text{-R}}$. The antisymmetric Dzyaloshinski-Moriya interaction is responsible for the covert and overt magnetic orderings (A_y, F_z) due to small canting of the Fe^{3+} spins. Below T_{N1} , the already ordered Fe^{3+} moments

*vivek.malik@ph.iit.ac.in

in most of the orthoferrites (except LaFeO_3) change their direction cooperatively as a function of temperature while maintaining the G-type antiferromagnetic structure. This phenomenon is called spin reorientation. Initially, it was proposed that the temperature dependence of the anisotropic part of the R^{3+} - Fe^{3+} exchange interaction leads to the observed spin reorientation in orthoferrites [27]. Later Yamaguchi *et al.* [25] established that the antisymmetric and anisotropic-symmetric parts of R^{3+} - Fe^{3+} exchange interactions are primarily responsible for the spin reorientation in orthoferrites. In addition to the spin reorientation, R^{3+} - Fe^{3+} exchange interactions also affect the magnetization of the rare-earth sublattice. The rare-earth moments can be aligned (polarized) via two different mechanisms: (1) the rare-earth polarization induced by the antisymmetric and anisotropic-symmetric R^{3+} - Fe^{3+} exchange interactions, which cause alignment of the rare-earth moments into a symmetry compatible with the magnetic ordering of Fe^{3+} sublattice, and a long coherence among such polarized moments can be observed by neutron diffraction or other techniques usually below 20–30 K, and (2) independent long-range antiferromagnetic order of the rare-earth moments, by virtue of the R^{3+} - R^{3+} interactions, into a symmetry different from the one induced by the R^{3+} - Fe^{3+} interactions. Henceforth, in this work, types (1) and (2) of the arrangement of the rare-earth moments shall be described as polarization and ordering of the rare-earth moments, respectively.

NdFeO_3 is one of the most studied orthoferrite compounds for magnetic ordering and the spin reorientation process [16,22,23,25,26,28–33] in which the Fe^{3+} spins undergo a continuous $\Gamma_4 \rightarrow \Gamma_2(F_x, C_y, G_z)$ reorientation between 200 and 150 K [29,31,34]. In the Γ_2 magnetic structure, the crystallographic c axis is the easy axis of the ordered Fe^{3+} spins in a basic G-type antiferromagnetic configuration along with ferromagnetic F_x and antiferromagnetic C_y configurations due to overt and covert canting of the spins [24,25]. The anisotropic and antisymmetric parts of the $\text{Nd}^{3+} - \text{Fe}^{3+}$ interactions, which causes the $\Gamma_4 \rightarrow \Gamma_2$ -type spin reorientation, also leads to gradual polarization of the Nd^{3+} magnetic moments. The long-range polarization of the Nd^{3+} moments is observed in neutron diffraction experiments below 20 K [26,30,35]. In most of the orthoferrites (except DyFeO_3), the R^{3+} moments usually order in a structure which is symmetry-compatible with the G-type arrangement of Fe^{3+} spins [25]. For instance, in NdFeO_3 , the Nd^{3+} moments polarizes as c_y^R , compatible to the Γ_2 representation of Fe^{3+} spins [26,30,35]. At the lowest temperatures (usually below 2 K) the $\text{Nd}^{3+} - \text{Nd}^{3+}$ interactions begin to supersede the $\text{Nd}^{3+} - \text{Fe}^{3+}$ interactions, resulting in long-ranged independent antiferromagnetic ordering of the Nd^{3+} moments, which can be considered as a Landau-type second-order phase transition [36].

Another isostructural, but relatively less studied, orthoferrite, ErFeO_3 , shows magnetic properties similar to NdFeO_3 . Fe^{3+} spins in ErFeO_3 order as canted G-type antiferromagnet in Γ_4 representation below 620 K (T_{N1}) [22]. Between $\sim 100/110$ K and $\sim 80/90$ K, the Fe^{3+} spins undergo a $\Gamma_4 \rightarrow \Gamma_2$ -type gradual spin reorientation [37–41]. The isotropic and anisotropic Er^{3+} - Fe^{3+} exchange interactions result in gradual polarization of the Er^{3+} moments, which causes the spin reorientation of Fe^{3+} spins.

In the low-temperature phase (below 20 K), the magnetic arrangement of Fe^{3+} spins is more complex due to the influence of polarized Er^{3+} moments on Fe^{3+} magnetic structure. At 1.3 K, Er^{3+} moments are polarized in a magnetic structure given by c_z^R configuration [22]. At this temperature (1.3 K), Koehler *et al.* [22] proposed that the Fe^{3+} spins with a G-type antiferromagnetic structure are confined in the a - b plane. Based on neutron diffraction data at 1.5 K, Gorodetsky *et al.* [42] proposed the possibility of two of the Fe^{3+} magnetic structures below the observed polarization of Er^{3+} moments. The first magnetic structure is given by the mixed representation of G_{xy} , wherein Fe^{3+} spins are aligned in the ab plane at an angle of $33^\circ \pm 4^\circ$ with respect to the b axis. As per the second proposed magnetic structure, Fe^{3+} spins should order as a G-type structure in bc plane (G_{yz}) with the spins at an angle of $51^\circ \pm 8^\circ$ from the b axis. Based on magnetization and torque measurements of the same study [42], Gorodetsky *et al.* confirmed the existence of a G_{yz} magnetic structure for Fe^{3+} spins at $T < 4.5$ K. The low-temperature magnetic structure of Fe^{3+} moments remained unresolved for a long time. Recently, Deng *et al.* [8] confirmed with the help of neutron diffraction and symmetry analysis that the low-temperature magnetic structure of Fe^{3+} spins remains Γ_2 (F_x, G_z) below spin reorientation temperature. Additionally, Deng *et al.* also detected C_y (C_x in $Pnma$ space group) mode of $\Gamma_2(F_x, C_y, G_z)$ magnetic structure below 5 K, at which the Er^{3+} moments start to polarize in the long-range antiferromagnetic arrangement given by c_z^R (c_y^R in $Pnma$ space group) configuration [8,42]. Yokota *et al.* [11] observed the coexistence of ferroelectricity and magnetism in ErFeO_3 thin films by modification of structure from orthorhombic to hexagonal via yttria-stabilized zirconia substrate.

In the family of orthoferrites, the DyFeO_3 exhibits an exceptional trend in spin-reorientation and rare-earth ordering [10,37,43–46]. Below T_{N1} (~ 650 K), the Fe^{3+} moments order with a structure given by Γ_4 representation. However, near ~ 35 K, a $\Gamma_4 \rightarrow \Gamma_1(A_x, G_y, C_z)$ -type spin reorientation occurs where the antiferromagnetic axis (b axis) becomes parallel to the Dzyaloshinsky-Moriya vector and weak ferromagnetic component cease to exist due to a pure uncanted antiferromagnetic structure [43,44]. This abrupt transition, also known as the Morin transition, is unique for DyFeO_3 in the family of rare-earth orthoferrites [23,37,43,47,48].

Below $T_{\text{N2}} \sim 4$ K, due to the Dy^{3+} - Dy^{3+} exchange and dipole interactions, the Dy^{3+} moments order in a long-range antiferromagnetic configuration given by $\Gamma_5(g_x^R, a_y^R)$ where the moments make an angle of 30° with the b axis [23,43,49–51]. Isostructural Dy-based compounds *viz.*, DyAlO_3 [52] and DyCrO_3 [53], also order in the same configuration. Due to large single-ion anisotropy, the Dy^{3+} moments are confined to the a - b plane [54].

Prelorendjo *et al.* [44] also studied magnetic-field-induced spin reorientation in DyFeO_3 . At 4.2 K, $\Gamma_1 \rightarrow \Gamma_4$, $\Gamma_1 \rightarrow \Gamma_2$, and $\Gamma_1 \rightarrow \Gamma_4$ -type spin reorientations of the Fe^{3+} sublattice were observed in DyFeO_3 on application of external magnetic field along the b , a , and c axes of the crystal, respectively [44]. The ordering (g_x^R, a_y^R) of Dy^{3+} moments, is not symmetry compatible with the field-induced Γ_2 magnetic structure of the Fe^{3+} sublattice [48]. Coexistence of the two incom-

patible magnetic structures breaks the inversion symmetry, which is essential for a linear magneto-electric effect [48,55]. Experimentally, a linear magneto-electric tensor component with a value as large as 2.4×10^{-2} esu is observed below the Dy^{3+} antiferromagnetic ordering temperature [10]. Interestingly, large ferroelectric polarization along with magnetic ordering also is achieved by application of an external magnetic field along the c axis of DyFeO_3 [10,45,56]. Rajeswaran *et al.* [56] claimed to observe simultaneous ferroelectricity and weak ferromagnetism above the Morin transition temperature in polycrystalline DyFeO_3 . A recent study by Wang *et al.* [46] observed a long- to short-range ordering transition of Dy^{3+} concurrent to the magnetic field (along the c -axis) induced spin reorientation of the Fe^{3+} sublattice. The magnetic-field-induced short-range ordering of the Dy^{3+} moments is responsible for the observed multiferroic phase induced by external magnetic field [10,46].

Recently spin reorientation of the Fe^{3+} sublattice and rare-earth ordering in single-crystal DyFeO_3 was explored using spin Hall magnetoresistance (SMR) and the spin Seebeck effect of a thin Pt contact in Hall bar geometry [57]. A clear signature of the spin reorientation of the Fe^{3+} sublattice (Morin transition) was observed in the SMR signal. In addition to the usual antiferromagnetic ordering of Dy^{3+} moments at 4 K, a magnetic-field-induced ordering of Dy^{3+} is observed up to 23 K. Hoogeboom *et al.* [57] proposed that the additional Dy^{3+} magnetic ordering occurs due to the external magnetic field and Dy^{3+} - Fe^{3+} exchange interaction. Such an ordering might be also related to the magnetic-field-induced short-range ordering of the Dy^{3+} moments observed by Wang *et al.* [46].

In addition to the pure orthoferrites, doping and/or substitution at the Fe and/or R sites shows interesting variations in the structural, magnetic, and electronic properties, while the fundamental characteristic of orthoferrites is still retained [12,58–63]. For instance, substitution at the Fe site with Mn has been studied and resulted in a systematic decrease of the Néel temperature [58,63] and structural distortion due to the Jahn-Teller effect [14], and modifies the preferred direction of Fe^{3+} spins due to single-ion anisotropy of Mn^{3+} ions [58,64]. Substitution at the A site by another rare earth, however, does not affect the structural behavior and Néel temperature, but affects the spin reorientation and the rare-earth ordering/polarization. For instance, twofold spin reorientations are observed in single crystals of $\text{Dy}_{0.5}\text{Pr}_{0.5}\text{FeO}_3$ and $\text{Ho}_{0.5}\text{Dy}_{0.5}\text{FeO}_3$ with varying temperature and magnetic field [61,62]. However, in these cases, the nature of the rare-earth ordering/polarization and its effect on the spin reorientation is not known.

Considering the striking contrast in the nature of Fe^{3+} and R^{3+} -orderings in ErFeO_3 and DyFeO_3 , it would be interesting to explore the properties of $\text{Er}_{0.5}\text{Dy}_{0.5}\text{FeO}_3$ (EDFO). A complex interplay of the various exchange interactions between the $\text{Er}^{3+}/\text{Dy}^{3+}$ and Fe^{3+} sublattices along with the R^{3+} - R^{3+} exchange interaction is expected. Additionally, due to the large magnetic moments of both rare earths, the classical dipole interactions are expected to play a prominent role in determining the complex ground-state magnetic structure at the lowest temperature. Due to large differences in the nature of single-ion anisotropy of both rare-earth ions (Er^{3+} and

Dy^{3+}) which can compete with the exchange and dipolar interactions, it would also be interesting to establish whether the arrangement (independent ordering or polarization) of the rare-earth moments is long-range or the magnetic ground state turns into a spin glass. Additionally, the possibility of a magneto-electric effect is also worth exploring.

Thus, we have experimentally studied the bulk magnetization, heat capacity, neutron diffraction, and magneto-dielectric measurements of polycrystalline EDFO. Theoretically, density functional theory calculations are performed to understand the ground-state electronic structure and evaluate the various exchange interactions from the total energies of various possible magnetic configurations.

II. METHODS

A. Experimental

Polycrystalline samples of EDFO were synthesized using solid-state reaction method. Er_2O_3 , Dy_2O_3 , and Fe_2O_3 precursor powders were weighed in appropriate stoichiometry and ground in an agate mortar for 12 hr. The steps involved calcination at 1200 °C for 24 hr, followed by heating at 1350 °C for 24 hr with intermediate grinding. Crystal structure of the sample was identified using a Bruker D8 two circle powder x-ray diffractometer with $\text{Cu } K_\alpha$ source. Bulk magnetization measurements were performed using a SQUID magnetometer of Quantum Design Inc.'s Magnetic Properties Measurement System-XL (QD-MPMS-XL) and the vibrating sample magnetometer option of Quantum Design Inc.'s Dynacool Physical Properties Measurement System (QD-PPMS). Zero-field-cooled (ZFC) and field-cooled (FC) magnetization measurements were carried out from 300 to 2 K in the presence of 0.01 and 0.1 T magnetic field. M - H isotherms were measured at various temperatures between 300 and 5 K. Using custom-designed probe for the QD-PPMS and Hioki EIM3536 LCR meter, magneto-dielectric studies were carried out in the temperature range of 300–2 K, at frequencies ranging from 1 to 500 kHz in the external magnetic field of 0, 0.1, and 1 tesla (T). Heat capacity measurements were performed using the QD-PPMS with ^3He option in the temperature range 20–0.4 K and magnetic field values of 0, 2, and 5 T. Powder neutron diffraction studies in zero magnetic field were carried out at various temperatures between 300 and 1.5 K to identify the crystal as well as magnetic structure and their evolution as a function of temperature. The neutron diffraction measurements were performed at the powder diffractometer G-41-I ($\lambda = 2.4206 \text{ \AA}$) at LLB, Saclay, France. The Rietveld analysis of the diffraction data was performed using the FullProf suite of programs [65,66]. Magnetic structures were determined using the irreducible representations from BasIreps [67].

B. Theoretical

The electronic structure of EDFO was studied using density functional theory implemented in the Vienna *ab initio* simulation program (VASP), which uses the projector augmented wave (PAW) method [68]. Calculations were performed using the Perdew-Burke-Ernzerhof (PBE) -based generalized gradient approximation (GGA) [69] and GGA+ U [70]. A cutoff energy of 500 eV was used in the expansion of

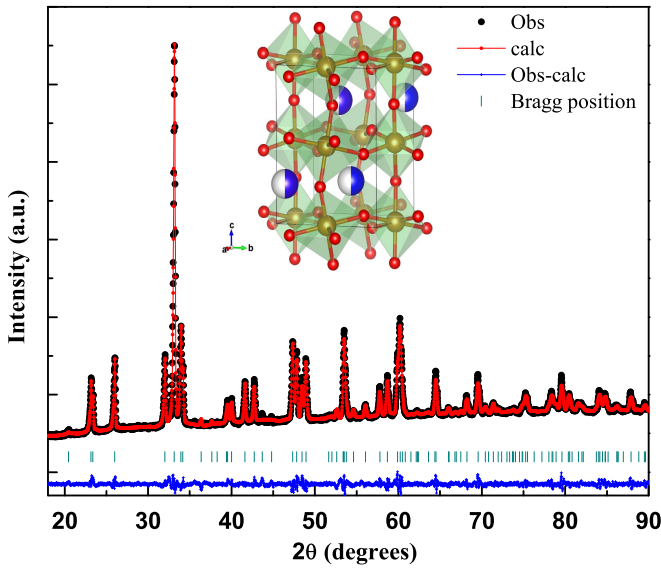


FIG. 1. Observed and refined x-ray diffraction pattern of EDFO at room temperature. We also show the unit cell of EDFO, wherein the Er and Dy atoms occupy same crystallographic site. The Er/Dy, Fe, and O atoms are represented by silver/blue, green, and red spheres, respectively, in the unit cell.

the plane waves. As shown in the inset of Fig. 1 and Fig. 11, an unit cell containing 4 formula units of EDFO is considered in our calculations. The structure was relaxed keeping the Er/Dy $4f$ electrons as core electrons. Ionic positions were relaxed until the forces on the ions are less than $0.1 \text{ meV } \text{Å}^{-1}$. For the electronic self-consistent calculations, the Er/Dy $4f$ electrons

were treated as valence electrons. We have considered following orbitals in the valence band for each atom: Fe: $3d$, $4s$, O: $2s$, $2p$, and Er/Dy: $4f$, $5p$, $5d$, $6s$. A $6 \times 6 \times 6$ Monkhorst-Pack k -mesh centered at the Γ point in the Brillouin zone was used for performing the Brillouin zone integrations. To establish the nature of the ground-state magnetic order, non-collinear calculations were performed with the inclusion of spin-orbit coupling within GGA+U+SO approximation.

III. EXPERIMENTAL RESULTS

A. Structural characterization

Figure 1 shows the room-temperature powder x-ray diffraction pattern for EDFO. The pattern is refined with the Rietveld method using the FullProf program. The pattern is refined to a single phase, with no trace of any impurity or unreacted phases. The compound crystallizes in the orthorhombic $Pbnm$ space group. At room temperature, the estimated lattice parameters are $a = 5.2793(5) \text{ Å}$, $b = 5.5835(6) \text{ Å}$, and $c = 7.6011(6) \text{ Å}$. The lattice (structural) parameters were also extracted from neutron powder diffraction patterns collected between 300 and 1.5 K. In Figs. 2(a)–2(c) the temperature variation of the three lattice parameters is shown. As expected, a , b , and c continuously decrease from 300 till 100 K. Further till 10 K, a and c decrease gradually with temperature, while b shows a “hump”-like feature between 50 and 10 K. Below 5 K we observe a sharp increase in all the three lattice parameters with a maximum around 2 K. The temperature variation of unit cell volume V [Fig. 2(d)] is similar to that of a and c , with a slope change below 100 K. In Fig. 2(e), we observe a sharp increase in volume with a maximum

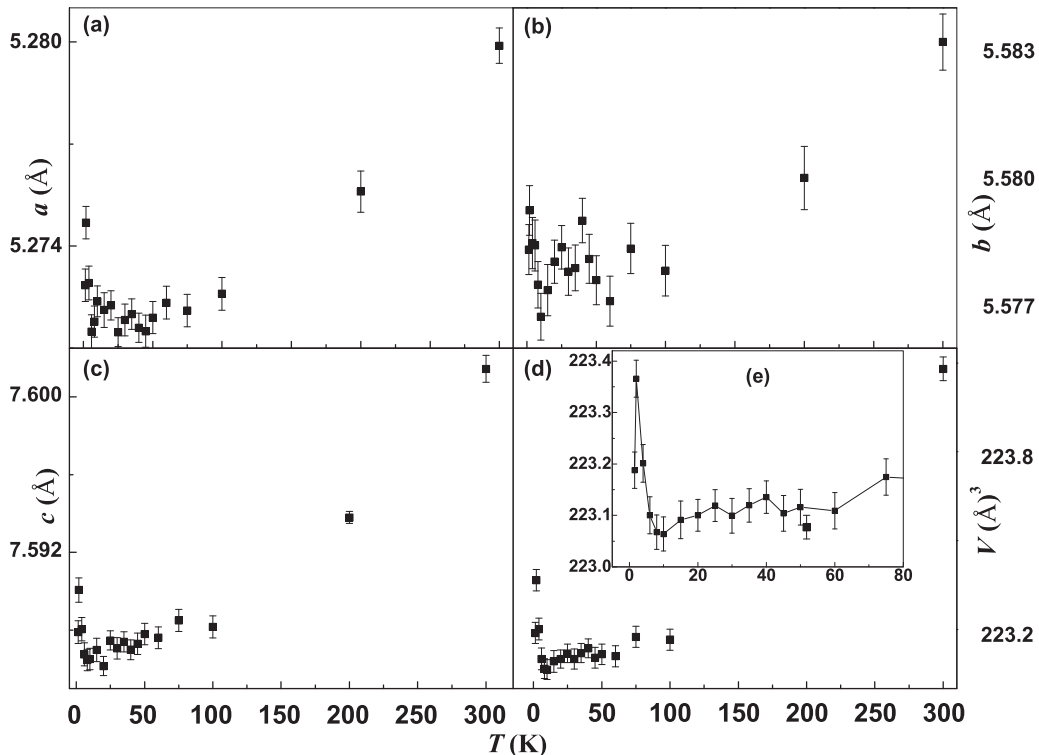


FIG. 2. [(a)–(c)] Temperature variation of lattice parameters, (d) unit cell volume of EDFO, and (e) anomalous rise in volume below 10 K.

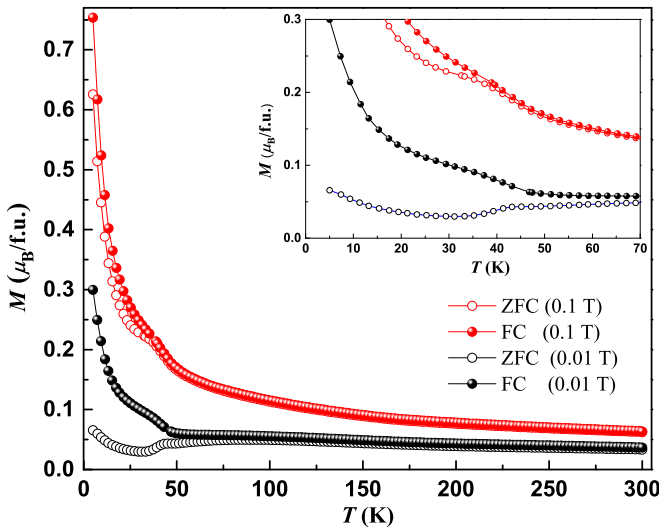


FIG. 3. ZFC-FC magnetization of EDFO at (a) 0.01 T and (b) 0.1 T. The inset shows enlarged portion of the graph below 70 K.

value at 2 K. In the absence of structural transformation, the “isotropic” negative thermal expansion effects may be considered as magneto-elastic or magneto-volume effect [71]. The anomalous negative thermal expansion is found to be associated with the long-range arrangement of rare-earth moments.

B. Magnetic properties

1. DC magnetization

Figure 3 shows the temperature-dependent zero-field-cooled (ZFC) and field-cooled (FC) magnetization measurements for EDFO from 2 to 300 K at magnetic fields of 0.01 and 0.1 T. At 300 K, EDFO is expected to be antiferromagnetically ordered in $\Gamma_4(G_x, A_y, F_z)$ magnetic structure, due to which we observe a small difference in the ZFC and FC magnetization. The spin reorientation of Fe^{3+} spins begins below $\sim 100/110$ K in ErFeO_3 [37–41]. Unlike ErFeO_3 , the signature of spin reorientation in EDFO appears below 70 K, indicated by the increase in bifurcation between ZFC-FC magnetization (in 0.01 T) as seen in Fig. 3. Near $T \sim 45$ K, the ZFC magnetization shows a drop, whereas the FC magnetization increases in a continuous manner with a change in slope near 15 K. This change in slope might be related to the polarization of Dy^{3+} moments, observed in neutron diffraction measurements in this work and observed earlier by Hoogeboom *et al.* [57] in SMR measurements. Below 25 K, the ZFC magnetization rises again, similar to ErFeO_3 [72]. Unlike DyFeO_3 , signature of a clear Morin-like transition is not observed in EDFO [45]. The ZFC-FC measurements for 0.1 T are also shown in Fig. 3. With a decrease in temperature, the ZFC and FC curves for 0.1 T show a continuous increase with a small slope change near 45 K.

The isothermal field variation of magnetization for various temperatures is shown in Fig. 4. At 300 K, the M - H curve shows a typical hysteresis loop of a canted antiferromagnet with a coercivity of nearly 0.2 T, confirming the weak ferromagnetism in EDFO. At 50 and 30 K, the M - H isotherm loops have relatively narrower hysteresis loops with an almost

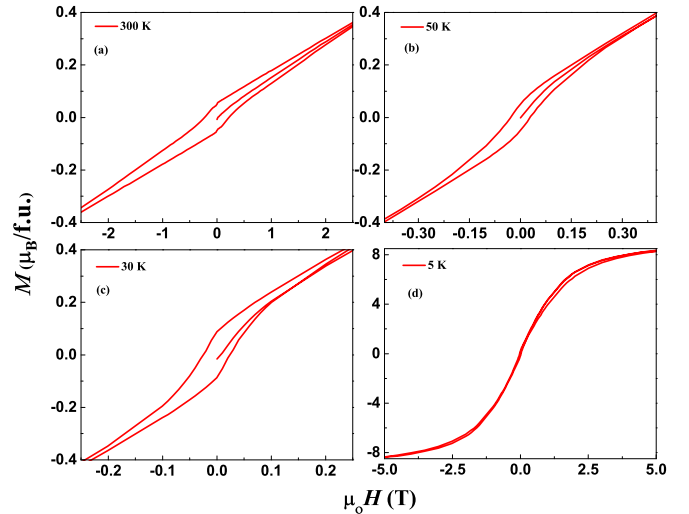


FIG. 4. M - H isotherms of EDFO at various temperatures.

linear magnetization at higher magnetic fields. The slope of linear magnetization at higher fields, which increases with decreasing temperature, is due to the development of the paramagnetic moment of both rare-earth ions [72]. At 5 K, the nonlinear behavior of the magnetization, at higher magnetic field, suggests polarization of the R^{3+} moments. In a magnetic field of 5 T, the magnetization attains a near-saturation (M_{sat}) value of nearly $8.4 \mu_B$. Both Er^{3+} and Dy^{3+} ions have a ground-state angular momentum quantum number $J = 15/2$, and their corresponding magnetic moments are $\sim 9.5 \mu_B$ and $\sim 10.6 \mu_B$, respectively. Magnetization studies on single crystals of DyFeO_3 reveal that the magnetic moment along the b axis attains a maximum value of nearly $9 \mu_B$, while a total magnetization of $10.6 \mu_B$ is obtained. Similarly, in ErFeO_3 , the total magnetic moment reaches a value of $7.6 \mu_B$ in a magnetic field of 5 T [73]. Thus the value of M_{sat} in EDFO lies between that of the corresponding parent compounds.

2. Magnetic neutron diffraction

In this section, the magnetic structures of EDFO obtained from neutron diffraction data is discussed. At 300 K (pattern not shown), we observe the structurally forbidden (101) and (011) magnetic peaks associated with G-type magnetic ordering of the Fe^{3+} spins. The neutron diffraction patterns obtained at 200, 45, and 20 K are shown in Figs. 5(a), 5(b), and 5(c). The magnetic peaks (011) and (101) correspond to ordering vector, $\vec{k} = (0, 0, 0)$. A ratio of nearly 1/3 between the intensities of (101) and (011) peaks confirms that the Fe^{3+} spins are arranged as G_x in the Γ_4 magnetic structure at 200 K [74]. Between 200 and 100 K, the ratio between the peaks remain nearly constant, while the absolute values of the intensity increase. Below 75 K, we observe relative increase in the intensity of (101) peak in comparison to the (011) peak, which indicates the onset of spin reorientation (data not shown). As shown in Fig. 5(b), at 45 K, the intensity of (011) peak is approximately twice in comparison to the intensity of (101) peak. Such intensity ratio suggests that a mixed magnetic structure, $G_{xz}(\Gamma_4 + \Gamma_2)$, exists at 45 K. The changes in intensity ratio of (101) and (011) peaks are

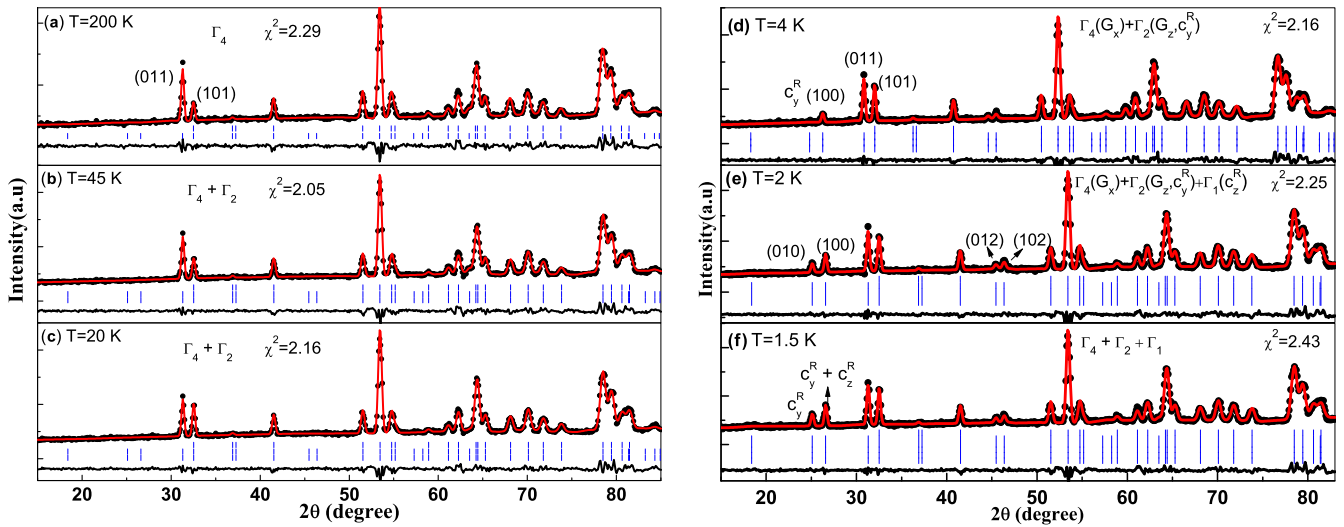


FIG. 5. Neutron powder diffraction pattern and refinements of EDFO at 200, 45, and 20 K (left panel) showing the systematic evolution of intensity of (011) and (101) magnetic peaks. In the right panel, patterns and refinement for 4, 2, and 1.5 K are shown. Additional magnetic peaks arising due to ordering of $\text{Er}^{3+}/\text{Dy}^{3+}$ moments are marked.

much more gradual than the previously studied mixed doped orthoferrite, $\text{Nd}_{0.5}\text{Dy}_{0.5}\text{FeO}_3$ [75].

Equal intensity ratio between (101) and (011) peaks is required for a pure $\Gamma_2(G_z)$ magnetic structure [74]. As evident from Fig. 5(c), the intensity of (101) and (011) peaks is not equal, hence the spin reorientation transition does not complete even at 20 K. In Figs. 5(d), 5(e), and 5(f), the neutron diffraction patterns for 4, 2, and 1.5 K are shown. As shown in Figs. 5(d), 5(e), and 5(f), the intensity ratio of (011) and (101) peaks remain slightly higher than 1 indicating presence of a mixed magnetic structure of Fe^{3+} sublattice down to the lowest measured temperature (1.5 K).

Below 10 K, additional peaks near 26° and 45° develop. In the $Pbnm$ space group the peak at 26° can be indexed to (100), while the peaks near 45° can be indexed to (012) and (102). All the three peaks are structurally forbidden in $Pbnm$ space group. Development of additional peaks can be attributed to onset of a long-range polarization (arrangement/coherence) of rare-earth ordering. With a decrease in temperature, the intensity of (100), (012), and (102) magnetic peaks increases in a systematic manner. At 2 K, an additional magnetic peak corresponding to (010) reflection appears, along with a sudden increase in intensity of (100) and (012)/(102) peaks related to rare-earth moments and (101) peak related to Fe^{3+} sublattice ordering. The magnetic peaks that develop below 10 K can also be indexed to $\vec{k} = (0, 0, 0)$.

In Fig. 6(a) the temperature variation of the integrated intensities of the (011) and (101) magnetic peaks is shown for temperature range from 300 till 1.5 K. Below 75 K, the intensity of (011) peak decreases, while that of (101) peak increases in systematic manner. Such a variation of magnetic peak intensity confirms the initiation of the spin reorientation at 75 K. This trend persists till 25 K, though they never cross over, which is a signature of complete reorientation. In Fig. 6(b) the enlarged version of intensity variation is shown between 15 and 1.5 K. Below 15 K, the (011) peak shows a gradual increase till 4 K, while that of the (101) peak remains nearly constant with small fluctuations till 4 K. The intensity

of the (101) peak increases considerably below 4 K. Hence, the ratio of (011) and (101) intensity decreases below 4 K.

Additionally, Fig. 6(b) shows the rise in intensity of the (100) and (010) peaks, associated with long-range polarization of R^{3+} moments. Between 10 and 4 K, the (100) peak shows a gradual rise in intensity. However, the (100) peak, similar to the (101) peak, shows a “discontinuous jump” in intensity at 4 K, which is accompanied by sudden development of the (010) peak. The overall variations in intensity clearly suggest coexistence of the multiple magnetic structures of Fe^{3+} and R^{3+} sublattices.

The nature of the multiple magnetic phases in EDFO is understood in detail from magnetic structural refinements using representational analysis [76]. The Fe atom occupies the 4b Wyckoff position, while the R atoms occupy the 4c sites. The Fe^{3+} spins can arrange in four possible magnetic representations (Shubnikov magnetic space group) $\Gamma_1(Pbnm)$, $\Gamma_2(Pbn'm')$, $\Gamma_3(Pb'nm')$, and $\Gamma_4(Pb'n'm)$. In Bertraut’s notation [24], the three spin components for each representation (Γ_1 to Γ_4) in Cartesian form are written as (A_x, G_y, C_z) , (F_x, C_y, G_z) , (C_x, F_y, A_z) , and (G_x, C_y, F_z) , respectively.

In EDFO, the magnetic structure of the Fe^{3+} sublattice belongs to Γ_4 representation from 300 to 75 K, which is in agreement with the general behavior of orthoferrites.

Based on intensity ratios of peaks, the spin reorientation transition starts to occur at 75 K similar to ErFeO_3 . Below 75 K, the magnetic structure is refined as a mixed structure given by $\Gamma_4 + \Gamma_2$ representations. The refinements indicate that the spin reorientation in EDFO is of the $\Gamma_4 \rightarrow \Gamma_2$ type, which is the usual second-order reorientation observed in various orthoferrites. In the temperature range below 60 K, we do not find a signature of $\Gamma_4 \rightarrow \Gamma_1$ abrupt transition as observed in DyFeO_3 . However, the $\Gamma_4 \rightarrow \Gamma_2$ reorientation is not complete even at 1.5 K, the lowest measured temperature.

The rare-earth moments, due to their lower site symmetry, can arrange in eight possible representations labeled Γ_1 to Γ_8 [25]. As shown in Fig. 6(b), below 10 K, the (100) magnetic peak starts to originate near the 26° value of 2θ diffraction

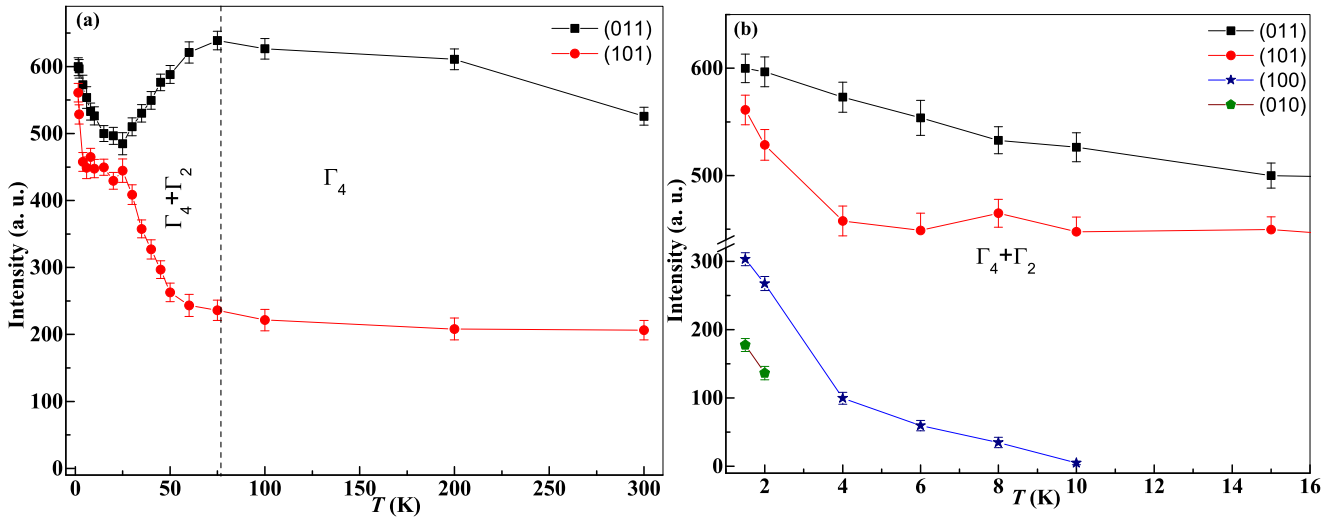


FIG. 6. (a) Temperature variation of intensity of various magnetic peaks between 300 and 1.5 K. (b) Temperature variation of intensity of various magnetic peaks below 15 K. The development of peaks due to R^{3+} ordering and anomalous rise in the intensity of (101) magnetic peak below 4 K is highlighted.

angle. From representational analysis, the (100) peak associated with the long-range polarization of the $\text{Er}^{3+}/\text{Dy}^{3+}$ moments corresponds to the symmetry of the c_y^R magnetic structure, which belongs to the Γ_2 representation. The corresponding magnetic moment is denoted as m_y^R . At 2 K, the sudden development of the (010) peak corresponds to the arrangement of the $\text{Er}^{3+}/\text{Dy}^{3+}$ moments in the c_z^R -type magnetic structure, which belongs to the Γ_1 representation. The corresponding magnetic moment is denoted as m_z^R . The c_z^R arrangements of Er^{3+} moments were also observed in ErFeO_3 [8,42]. In ErFeO_3 , the Fe^{3+} show a probable coexistence of Γ_1 and Γ_2 magnetic structures coinciding with c_z^R ordering of the Er^{3+} moments [42]. Similarly, at 1.5 K, due to the c_z^R -type polarization of $\text{Er}^{3+}/\text{Dy}^{3+}$ moments in EDFO, development of the Γ_1 structure for the Fe^{3+} spins is also expected in addition to combined Γ_{24} structure [8]. The signature of the Γ_1 magnetic structure of Fe^{3+} spins can be determined from the increase in intensity of the (101) peak below 4 K as indicated in Fig. 6(b). However, to confirm this by refinement, the data at 2 and 1.5 K are refined to combinations of Γ_{24} as well as $\Gamma_{24}+\Gamma_1$ structures. At 2 K, the fitting does not converge with inclusion of three phases. However, at 1.5 K the goodness of fit is equal in both cases. In Fig. 7 we show a fitting in Γ_{24} (upper panel) and $\Gamma_{24}+\Gamma_1$ (lower panel), highlighting the (011) and (101) peak. Considering all three representations of Fe^{3+} ($\Gamma_{24}+\Gamma_1$), the fitting quality seems to be slightly better. However, inclusion of the Γ_1 structure in our refinement does not lead to any observable changes or improvement in the quality of refinement. Thus, though the coexistence of Γ_1 with the Γ_{24} phase is plausible due to the compatible symmetry c_z^R arrangement of $\text{Er}^{3+}/\text{Dy}^{3+}$ moments only with the G_y arrangement of Fe^{3+} spins [8], the presence of the Γ_1 structure, at 1.5 K, can be neither confirmed nor ruled out from the refinement of our data.

The temperature variation of the magnetic moments for the Fe^{3+} and R^{3+} moments for different representations is shown in Fig. 8(a). The values of the total magnetic moment

of Fe^{3+} is nearly $3.2 \mu_B$, which is lower than the theoretical expected value of $5 \mu_B$. Such reduction might be due to effects of covalency, disorder and the polycrystalline nature of our samples. From 300 to 75 K, we observe a small increase in the magnetic moment (M_x) associated with G_x configuration. With the onset of spin reorientation, there is a decrease in M_x , while correspondingly the M_z shows an increase. Below 20 K both M_x and M_z remain nearly constant with small fluctuations as shown in Fig. 8(b). Also, as seen in Fig. 8(b), from 10 to 1.5 K m_y^R shows a gradual increase, while m_z^R shows a sudden development at 2 K. The m_y^R and m_z^R moments attain values of nearly 1.4 and $1.7 \mu_B$ respectively, resulting in a total rare-earth sublattice moment of $2.4 \mu_B$ at 1.5 K. The possible M_y component of the Fe^{3+} moments which exists only at 1.5 K has a much larger error bar as shown in Fig. 8(b).

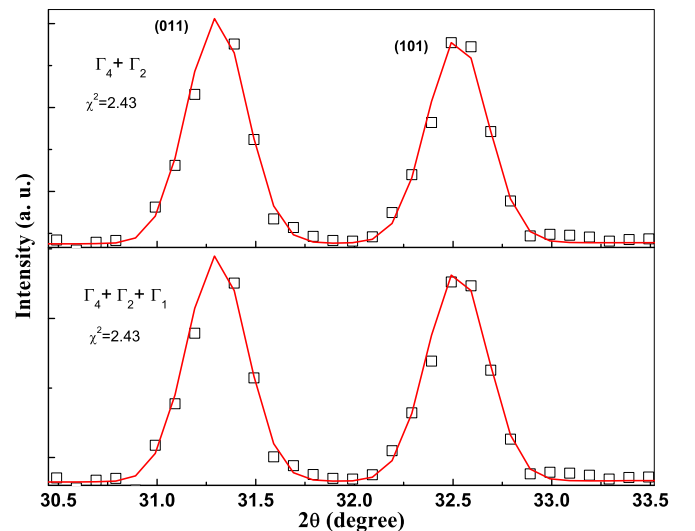


FIG. 7. (011) and (101) magnetic Bragg peaks showing results of fitting by $\Gamma_4+\Gamma_2$ (upper panel) and $\Gamma_4+\Gamma_2+\Gamma_1$ (lower panel) magnetic structures of the Fe^{3+} spins.

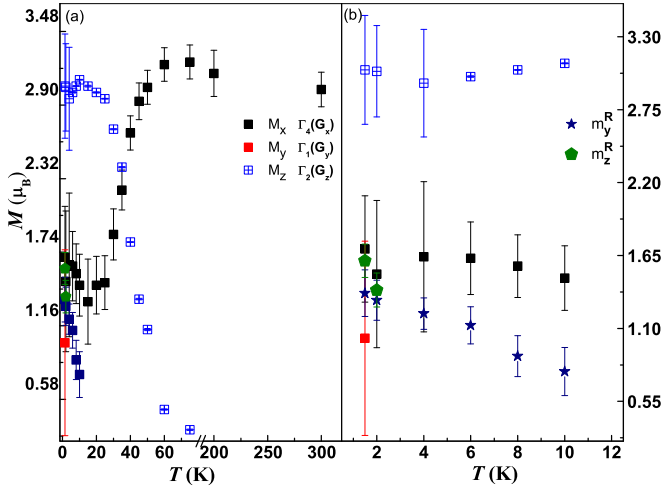


FIG. 8. (a) Temperature variation of magnetic moment of Fe^{3+} and $\text{Er}^{3+}/\text{Dy}^{3+}$ spins from 1.5 to 300 K for the various magnetic structures. (b) The variation of magnetic moments in the temperature range from 10 to 1.5 K. The arrow shows the discontinuity/sudden rise of m_z^R .

In Table I we list the magnetic configurations of EDFO at various temperatures. The magnetic configurations of the parent compounds of ErFeO_3 and DyFeO_3 are also listed as a reference at the corresponding temperatures. The Fe^{3+} and $\text{Er}^{3+}/\text{Dy}^{3+}$ magnetic structure of EDFO and its variation is closer to ErFeO_3 rather than DyFeO_3 . The magnetic structures of EDFO at 50, 4, and 1.5 K depicting the Fe^{3+} and $\text{Er}^{3+}/\text{Dy}^{3+}$ moments are shown schematically in Figs. 9(a)–(c).

3. Specific heat

The heat capacity C_p of EDFO for 0, 2, and 5 T are shown in Fig. 10 from 0.4 to 20 K. The zero field heat capacity shows a rise below 8 K with a peak at 2.2 K. The λ -shaped anomaly associated with second-order phase transition, seen in DyFeO_3 [49] at 4.2 K, is absent in EDFO. Independent magnetic ordering of the R^{3+} ions is absent till 0.4 K, which is in agreement with our neutron diffraction results. The feature observed in EDFO is similar to the peak observed in ErFeO_3 due to the Schottky effect [77].

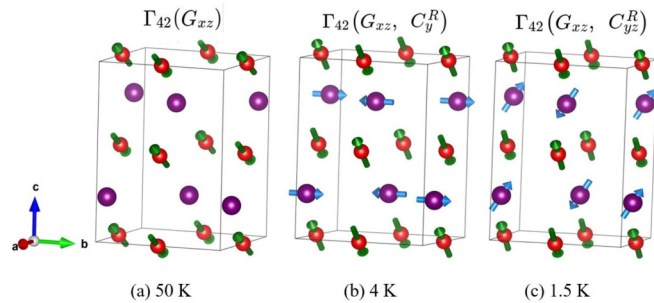


FIG. 9. Magnetic structure of EDFO at (a) 50 K: G_x, G_z arrangement of Fe^{3+} spins, (b) 4 K: (G_x, G_z, C_y^R) , and (c) 1.5 K: (G_x, G_z, C_y^R, C_z^R) . Red spheres represent Fe atoms, violet spheres represent Er/Dy atoms.

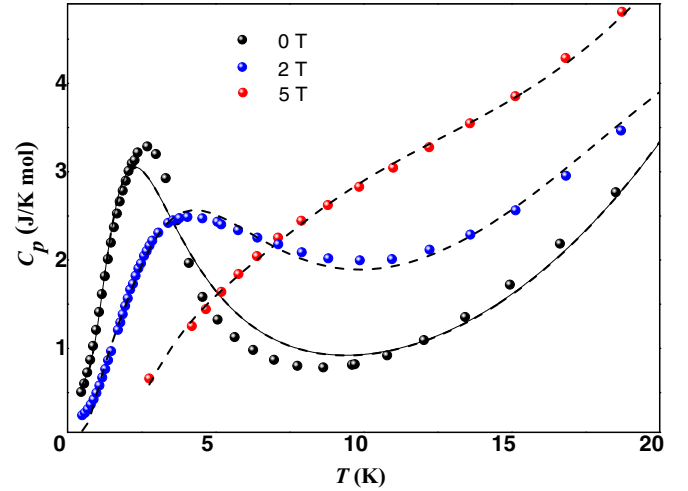


FIG. 10. The low-temperature specific heat of EDFO for 0, 2, and 5 T. The dashed and solid lines show the fitting of specific heat to Schottky and lattice terms.

In EDFO, the Er^{3+} and Dy^{3+} being odd-electron systems, the ground state of each ion is a Kramer's doublet split by molecular, exchange, and dipole fields. Thus the low-temperature peak in C_p is due to the splitting of the ground-state doublet of both the rare-earth ions. To extract information about the splitting of the doublets, the specific heat is fitted in the temperature range 0.4–20 K as a sum of “two-level” Schottky terms corresponding to both the rare-earth ions and the T^3 lattice term as

$$C_p = \frac{1}{2}R \sum_{i=1}^2 w_i \left(\frac{\Delta E_i}{k_B T} \right)^2 \frac{\exp\left(-\frac{\Delta E_i}{k_B T}\right)}{[1 + \exp\left(-\frac{\Delta E_i}{k_B T}\right)]^2} + B_3 T^3. \quad (1)$$

In Eq. (1) $\Delta E_1/k_B$ and $\Delta E_2/k_B$ correspond to the doublet splitting in each R^{3+} ion, while B_3 is the lattice term. A single energy splitting is insufficient to simulate the correct magnitude of the peak in C_p . From the fitting, the value $B_3 = 4.04 \times 10^{-4} \text{ J/mole-K}^4$ is obtained, which yields a Debye temperature of 457 K for EDFO. At 0 T, we obtain $\Delta E_1/k_B = 1.5 \text{ K}$ and $\Delta E_2/k_B = 5.6 \text{ K}$. These values are in good agreement with the optical spectroscopy studies on both parent compounds as discussed further.

Optical studies on ErFeO_3 revealed that the splitting of the ground-state doublet in the Γ_2 phase is nearly constant from 77 to 5 K with a value of 3.17 cm^{-1} (0.39 meV or 4.52 K) [78]. Similarly, above the Dy^{3+} ordering temperature, the splitting of the ground-state doublet in DyFeO_3 is nearly 1.5 cm^{-1} (0.185 meV or 2.14 K) within experimental resolution [79]. The splitting in both cases is attributed to the R^{3+} - Fe^{3+} interactions. Thus, the values of $\Delta E_1/k_B$ and $\Delta E_2/k_B$ in EDFO can be attributed to the doublet splitting in the Dy^{3+} and Er^{3+} ions, respectively. However, due to complex temperature dependence of ΔE , especially in the case of the doublet of the Er^{3+} ion [80], temperature-independent ΔE terms cannot satisfactorily fit the Schottky peak, especially for a zero field.

The C_p measured at 2 T, fitting Eq. (1) yields $\Delta E_1 = 5.9 \text{ K}$, while ΔE_2 increases to 26 K. At 5 T we obtain $\Delta E_1 = 13.6 \text{ K}$ and $\Delta E_2 = 34 \text{ K}$. Thus, the effect of magnetic field on the ground state of Er^{3+} is more drastic, indicating greater po-

TABLE I. Magnetic structural details of $\text{Er}_{0.5}\text{Dy}_{0.5}\text{FeO}_3$ from the present study and comparison with the literature for ErFeO_3 and DyFeO_3 . The “ \rightarrow ” and “ \sim ” denote a complete and incomplete reorientation, respectively.

Compound	$T_N > T > T_{SR}$	SR	$T_{SR} > T > T_R$	$T_R > T > 4\text{ K}$		$T = 1.5\text{ K}$		Reference
	Fe^{3+}	Type	Fe^{3+}	Fe^{3+}	R^{3+}	Fe^{3+}	R^{3+}	
$\text{Er}_{0.5}\text{Dy}_{0.5}\text{FeO}_3$	$G_x F_z$	$\Gamma_4 \sim \Gamma_2$	G_{xz}	G_{xz}	c_y^R	Model 1: G_{xz}	$c_y^R c_z^R$	This work
				—	—	Model 2: G_{xyz}	$c_y^R c_z^R$	This work
ErFeO_3	$G_x F_z$	$\Gamma_4 \rightarrow \Gamma_2$	$F_x G_z$	$F_x C_y G_z$	c_z^R			[8,22,37–42]
DyFeO_3	$G_x F_z$	$\Gamma_4 \rightarrow \Gamma_1$	G_y	G_{xy}	—	G_{xy}	$g_x^R a_y^R$	[10,23,37,43–46,50,51,54]

larizability due to external fields. The values of ΔE for both ions though obtained indirectly are close to the experimental splittings observed directly from Zeeman effect studies on both parent compounds [78,79,81].

IV. DFT CALCULATIONS

The magnetic structure of EDFO is also explored using density functional theory. In the $Pbnm$ structure, the Er and Dy atoms occupy the $8c$ sites in a random fashion. For computational purposes, we have considered two regular arrangements of Er and Dy atoms, *viz.*, the (111) and (001) arrangements [75]. In the (111) arrangement, the Er and Dy atoms are placed adjacent to each other. Thus each Er atom has six Dy atoms as nearest neighbors and vice versa. In the (001) arrangement, Er and Dy atomic planes are alternately stacked along the c axis [75].

For both cationic arrangements, structural relaxation of the orthorhombic unit cell has been performed using the experimental structural parameters obtained for 300 and 1.5 K. The structure was relaxed considering G-type magnetic ordering of the Fe^{3+} magnetic moments. The electronic self-consistent calculations were performed to obtain the total energies of various structural (cationic) and magnetic arrangements of EDFO, for which the Hubbard U on Fe and Er/Dy was incorporated. The Hubbard parameters $U = 8.5\text{ eV}$ and $J = 0.5\text{ eV}$ for Er and Dy; and $U = 5.0\text{ eV}$ and $J = 1\text{ eV}$ for Fe are used because these are the typical values used in previous literature for $4f$ states of rare-earth ion and $3d$ states of Fe in orthoferrites [34]. We have used $U_{\text{eff}} = U - J$ (Dudarev’s approach [82]), which is 8 eV for Er/Dy $4f$ states and 4 eV for Fe $3d$ states. The iterations were performed till an energy difference of 10^{-6} eV was achieved. Energetically, it is found that the (001) arrangement has lower energy as compared to the (111) arrangement. In the case of the Fe^{3+} sublattice, the lowest energy corresponds to G-type magnetic ordering, which is common in all orthoferrites [83].

The rare-earth ordering was probed for various non-collinear magnetic structures with the inclusion of the spin-orbit coupling within the GGA+U+SO approximation. We have considered two possible arrangements of the $\text{Er}^{3+}/\text{Dy}^{3+}$ moments, (1) c_y^R and (2) g_x^R . The Fe^{3+} spins were kept fixed in a G_z magnetic configuration in these calculations. As seen in Table II, c_y^R has a lower energy as compared to g_x^R in both cationic arrangements. The magnetic moment of Fe^{3+} obtained from DFT is $4.2\ \mu_B$, which is smaller than the free ion value of $5\ \mu_B$, though larger than the exper-

imentally obtained value. The reduction can be attributed to effects of hybridization with the O $2p$ bands. The spin magnetic moment values of Er^{3+} and Dy^{3+} are found to be $2.8\ \mu_B$ and $5\ \mu_B$, respectively. The corresponding orbital moment values are $5.0\ \mu_B$ and $4.1\ \mu_B$, thus yielding total magnetic moments of $7.8\ \mu_B$ and $9.1\ \mu_B$ for Er^{3+} and Dy^{3+} , respectively. These values match quite well with those reported in previous studies on DyFeO_3 and ErFeO_3 (see Table III).

Figures 11(a) and 11(b) show the the partial density of states of EDFO for (111) and (001) arrangements calculated within the GGA+U+SO approximation for noncollinear magnetic states shown in the inset. In both arrangements, a band gap of $\sim 2.2\text{ eV}$ is obtained. Just below the Fermi energy, the spectral character of DOS is mainly the combination of strongly hybridized Fe $3d$ and O $2p$ states. In both arrangements, the behavior of Fe $3d$ bands appears similar. However, the $4f$ states of Er and Dy show a slightly different behavior in these two arrangements. In (001) arrangement Er/Dy $4f$ states overlap more with each other than the same in the (111) arrangement in the energy range -3 to -5 eV below the Fermi level while the Fe $3d$ states are seen to hybridize with the Er $4f$ state in both arrangements in the energy range -6 to -7 eV below the Fermi level. Er and Dy $4f$ states show a sharp spectral feature with high intensity about -6 eV below the Fermi level.

The strengths of the magnetic exchange interactions between $\text{Er}^{3+}\text{-Er}^{3+}$, $\text{Dy}^{3+}\text{-Dy}^{3+}$, and $\text{Er}^{3+}\text{-Dy}^{3+}$ have been determined from our density functional theory calculations within the GGA+U approximation. Additionally, the strengths of $\text{Er}^{3+}/\text{Dy}^{3+}\text{-Fe}^{3+}$ exchange interactions are also determined. The differences in energies of ferromagnetic and antiferromagnetic arrangements are mapped to the Heisenberg Hamiltonian [83,89]. The calculations were performed on “artificial unit cells” using the experimental structure of 1.5 K,

TABLE II. Relative energies (in meV) for two main anti-ferromagnetic ordering with $\text{Er}^{3+}/\text{Dy}^{3+}$ magnetic moments in noncollinear arrangement calculated within GGA+U+SO approximation. The Hubbard parameters used are $U = 8.5\text{ eV}$ and $J = 0.5\text{ eV}$ for Er and Dy. The Fe^{3+} spins were fixed in the G_z antiferromagnetic arrangement.

Magnetic structure	Alternate (111)	Layered (001)
c_y^R	0	0
g_x^R	+62.8	+52.0

TABLE III. The various exchange interaction strengths in $\text{Er}_{0.5}\text{Dy}_{0.5}\text{FeO}_3$ obtained from DFT. Also listed from literature are the R - R and R -Fe interaction strengths of some of the parent orthoferrite compounds, obtained from various experimental techniques. Wherever applicable, the values are given in terms of fields as well as interaction energies for both cases: exchange and dipole interactions.

Compound	Magnetic moment of rare earth (μ_B)	Ions	Exchange energy/field (meV)/teslas	Dipole energy/field (meV)/teslas	Reference
$\text{Er}_{0.5}\text{Dy}_{0.5}\text{FeO}_3$	7.8(Er)	Er-Fe	2.886 meV		This work
	9.1(Dy)	Dy-Fe	0.019 meV		
		Er-Dy	1.381 meV		
		Er-Er	-0.037 meV		
		Dy-Dy	0.585 meV		
DyFeO_3	9.2 ± 1.0	Dy-Dy	0.07 meV		[43]
	9.2	Dy-Dy		0.56 T	[49]
		Dy-Fe	0.17 T		[79]
		Dy-Fe	6.5 ± 1.1 T		[44]
		Dy-Fe	0.1 T (isotropic)		[84]
		Dy-Fe	2.0 T		
ErFeO_3	5.8	Er-Er		0.5 T	[22]
	6.6 ± 0.2	Er-Fe		0.22 T (avg)	[78]
		Er-Fe	x 0.28 and 0.84 T	x 0.09 T	[81]
		Er-Fe	y 4.4 and 2.6 T	y 0.31 T	
		Er-Fe	x -2 T		
		Er-Fe	y -1 T		[85]
		Er-Fe	z -0.12 T		
GdFeO_3		Gd-Gd	0.005 meV		[86]
		Gd-Fe	0.008 meV		
		Gd-Fe	0.033 meV		[87]
		Gd-Fe	0.019 meV		[88]
NdFeO_3	<0.5	Nd-Fe	3 T		[22]
		Nd-Nd	0.075 meV		[36]
	0.66	Nd-Fe	6.6 T		[30]
					[26]

in which except for the selected Fe or Er/Dy atoms, the rest of the magnetic atoms are replaced by nonmagnetic atoms. Thus the Fe atom is replaced by Al, while both Er and Dy are replaced by La atoms, since La^{3+} ion is nonmagnetic [83].

From the calculations, it is found that the Dy^{3+} - Fe^{3+} interaction is the weakest, with a value of 0.019 meV, which is smaller than the single ion anisotropy of Dy^{3+} ion [48]. This is also consistent with previous studied by Zvezdin *et al.* [84]

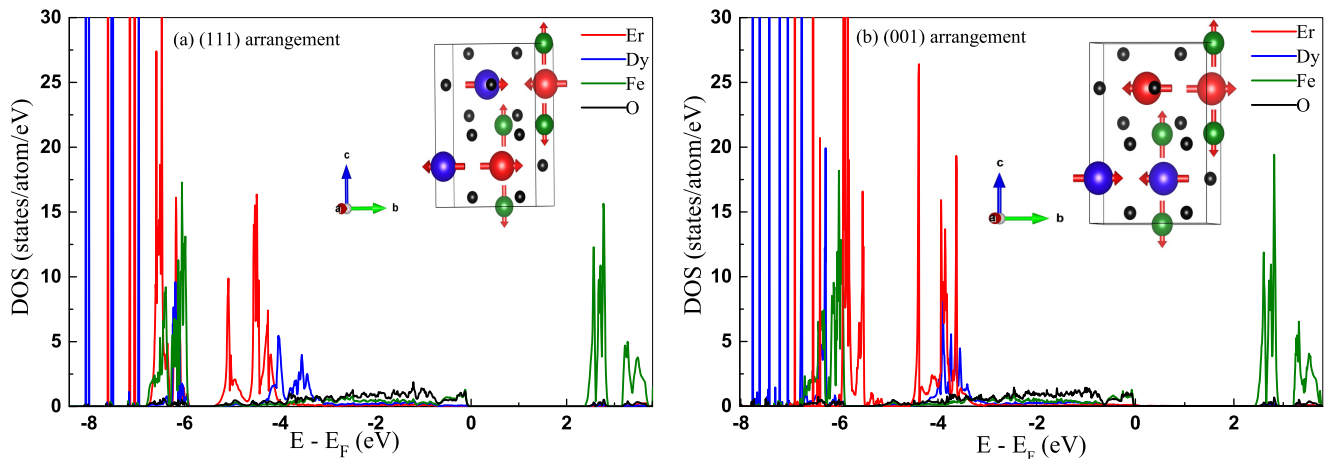


FIG. 11. Partial density of states(DOS) of EDFO for the (a) alternate (111) (b) layered (001) calculated within GGA+U+SO approximation with noncollinear spin arrangements of Er and Dy as shown in the inset.

on DyFeO₃ where it was observed that the isotropic part of the Dy³⁺-Fe³⁺ exchange interaction (which is calculated here) is usually compensated and attains a relatively smaller value of 0.1 T. The Er³⁺-Fe³⁺ interaction, with a much higher value of 2.88 meV (which is consistent with previous studies [81]), thus plays important role in the $\Gamma_4 \rightarrow \Gamma_2$ reorientation. Among the interaction strengths between the rare earths, the Dy³⁺-Dy³⁺, Er³⁺-Er³⁺, and Er³⁺-Dy³⁺ exchange interaction values are found to be 0.58, -0.037, and 1.38 meV, respectively (negative sign indicates AFM interaction). Experimental studies on DyFeO₃ indicate an ordering temperature of 3.5 K for the Dy³⁺ moments, while in DyAlO₃ and DyScO₃, the Dy³⁺ moments order at 4.5 K [52,54]. Berton *et al.* [49] have extracted an effective nearest-neighbor exchange J/k_B by considering an Ising model and simple cubic lattice to fit the experimental specific heat and rare-earth ordering temperature in DyFeO₃ and found it to be in the range 0.7–0.8 K. In our case, three types of R^{3+} - R^{3+} nearest-neighbor exchange interactions (Dy³⁺-Dy³⁺, Er³⁺-Er³⁺, and Er³⁺-Dy³⁺) are at play. Moreover, the Dy³⁺-Dy³⁺ exchange interaction is found to have values 0.58 meV in the ab plane and -1.21 meV along the c direction, respectively. Though the Dy³⁺-Dy³⁺ exchange interaction is found to be much larger ($J/k_B \sim 6.7\text{K}-14\text{K}$) in EDFO compared to that obtained by Berton *et al.* [49] in DyFeO₃, the presence of multiple exchange interactions and their competing nature can lead to a much lower ordering temperature in our system. The small size of the Er³⁺-Er³⁺ interaction further indicates that the Er³⁺ moments can be polarized by the molecular field of Fe, suppressing the independent ordering of Er³⁺ moments as in ErFeO₃. An appreciable value of Er³⁺-Dy³⁺ exchange interactions helps in establishing the long-range ordering by polarization of the Er/Dy sublattice below 10 K.

V. DISCUSSION

A. $\Gamma_4 \rightarrow \Gamma_2$ “incomplete” reorientation of Fe³⁺ spins

In the Γ_4 phase below the T_{N1} , due to the F_z component of Fe³⁺ spins, an effective molecular field along the z axis develops. Such an effective field induces a net polarization on the R^{3+} moments, which by symmetry, should align as f_z^R .

The Er³⁺-Fe³⁺ interactions are much greater than the Dy³⁺-Fe³⁺ interactions as seen in our first principles calculations and optical studies [78,79]. According to the effective field model by Yamaguchi *et al.* [48], the anisotropic-symmetric and antisymmetric parts of Er³⁺ and Fe³⁺ exchange interactions cause rotation of the Fe³⁺ spins below 75 K, resulting in the $\Gamma_4 \rightarrow \Gamma_2$ reorientation near 75 K. This behavior is identical to the reorientation in ErFeO₃ [42].

During reorientation, the spontaneous weak ferromagnetic component of Fe³⁺ moments changes from F_z to F_x . Due to two dissimilar rare-earth ions, a local variation in the exchange field develops in the system. The Dy³⁺ ions do not affect the spin reorientation to a large extent, since the smaller Dy³⁺-Fe³⁺ interaction does not play a major role. Thus, instead of reorientation occurring in a short interval of 10 K as in ErFeO₃ [42], a very gradual reorientation takes place in EDFO. This results in coexistence of $\Gamma_4(G_x, C_y, F_z)$ and $\Gamma_2(F_x, C_y, G_z)$ in the entire temperature range below

75 K, wherein F_z and F_x play a role similar to the external applied field.

The external field along various crystal axes causes spin reorientations in both parent compounds. However, compared to ErFeO₃ [73], the effect of the field is more drastic in DyFeO₃ at smaller fields. For a field along the a direction, above a critical field (of nearly 1–2 T), a $\Gamma_1 \rightarrow \Gamma_4$ transition is induced. A relatively small field along the c direction and b direction, $\Gamma_1 \rightarrow \Gamma_2$ reorientation is induced in DyFeO₃ [44]. The effective molecular fields along the a , b , and c directions eventually suppress the Morin transition in EDFO. At 50 K, coexistence of both magnetic structures exists as shown in Fig. 9(a), which persists till 1.5 K. We also explored the possibility of an additional magnetic phase Γ_1 in addition to the Γ_{24} at 1.5 K. Hence, the spin reorientation in EDFO can be considered to be an “incomplete reorientation.”

B. Polarization of rare-earth moments

1. Development of c_y^R arrangement of R^{3+} moments

Just as the predominant Er³⁺-Fe³⁺ interaction causes the $\Gamma_4 \rightarrow \Gamma_2$ reorientation, this also results in the polarization of the R^3 moments in the (f_x^R, c_y^R) configuration. The polarization of Er³⁺ moments is much easier as compared to the Dy³⁺ moments. Though the preferred arrangement of Dy³⁺ moments is (g_x^R, a_y^R) , this is actually the spin-flopped configuration of (f_x^R, c_y^R) with the energy difference smaller than the single-ion anisotropy of Dy³⁺ [48]. Thus the effective field along the x axis can also partially polarize the Dy³⁺ moments along with the Er³⁺ moments. Hence, at 4 K, Fe³⁺ spins are in the Γ_{42} configuration, and the R^{3+} moments are in the c_y^R configuration [Fig. 9(b)].

2. Development of c_z^R arrangement of R^{3+} moments

At 2 K, a sudden appearance of the c_z^R magnetic Bragg peaks occurs. As shown in Fig. 8(b), the magnetic moment (m_z^R) shows a sudden rise. The mechanism behind the sudden appearance of c_z^R and abrupt reorientation $G_x \rightarrow G_y$, which is a characteristic feature of ErFeO₃, is more complex to understand. In Fig. 9(c) we show the coexistence of c_y^R and c_z^R along with Fe³⁺ spins having (G_x, G_z) at 1.5 K. The mechanism behind the sudden appearance of a peak related to the c_z^R -type structure, which is a characteristic feature of ErFeO₃, is more complex to understand. In Fig. 9(c) at 1.5 K, we show the coexistence of magnetic structure of Er³⁺/Dy³⁺ and Fe³⁺ sublattices.

C. Symmetry of the rare-earth magnetic structure

The ground state of Dy³⁺ and of Er³⁺ ions, *viz.*, ${}^6H_{15/2}$ and ${}^4I_{15/2}$, respectively, is split by the monoclinic crystal field $[C_s(m)]$ into eight Kramer’s doublets [52,81]. Inelastic neutron studies reveal that the splitting between the ground state and first excited doublet of Er³⁺ is around 5.5 meV, while in the case of Dy³⁺ a separation of nearly 6.8 meV is observed. Below 50 K, only the lowest doublet is populated in both ions. Hence, the Er³⁺ and Dy³⁺ ions are described as “effective spin” $S_R = 1/2$ (R : rare earth) systems, which are twofold degenerate. The degeneracies of the ground state of

both ions are Zeeman split by an energy ΔE due to external field as well as internal molecular fields \vec{H}_{eff} due to R^{3+} - Fe^{3+} , R^{3+} - R^{3+} , exchange, and dipolar interactions. The coupling of the Er^{3+} and Dy^{3+} “spins” to the effective fields occur via the anisotropic “ \mathbf{g} ” tensor [78,79].

Mean-field studies pertaining to rare-earth magnetism in $R\text{CrO}_3$ ($R = \text{Nd, Er}$), show that temperature evolution of the magnetic moment of R^{3+} and ΔE are related in a self-consistent manner. The sublattice magnetization of R^{3+} is defined as $m^R = 1/2g_y\mu_B N \langle S_R \rangle$; where the thermal average of the R^{3+} “spin” is related to the doublet splitting as $\langle S_R \rangle = B_S(\Delta E/k_B T)$. Here $B_S(x)$ is the Brillouin function, which becomes $\tanh(x)$ for $S_R = 1/2$ [90].

Optical spectroscopy and mean field analysis on NdCrO_3 and ErCrO_3 show that, below T_{N1} , ΔE is proportional to temperature-dependent sublattice magnetization of Cr^{3+} spins $\langle S \rangle/S$ ($S = 3/2$ for Cr^{3+}). However, below the spin reorientation temperature (T_{SR}), when the R^{3+} - R^{3+} interactions become nonnegligible, ΔE is proportional to the sum of (1) sublattice magnetization of Cr^{3+} spins and (2) $\tanh[\Delta E(\vec{H}, T)/2k_B T]$ [80,90].

In EDFO, the situation is more complex, since the temperature dependence of ΔE , is different for the Er^{3+} and Dy^{3+} ions. Thus, in EDFO, the variation in m_y^R can be attributed to sum of the three terms, (1) Fe^{3+} sublattice magnetization, (2) $\tanh(\Delta E_{\text{Er}}(\vec{H}, T)/2k_B T)$, and (3) $\tanh(\Delta E_{\text{Dy}}(\vec{H}, T)/2k_B T)$. In EDFO, even above 75 K, the Fe^{3+} spins have attained their maximum value. In the range 1.5–10 K the net sublattice magnetic moment of Fe^{3+} is nearly constant. The eventual rise in the intensity of the c_y^R peak below 10 K can be attributed to the interaction between the R^{3+} ions along with a stronger Er^{3+} - Fe^{3+} exchange interaction. In view of the negligible Er^{3+} - Er^{3+} exchange interactions, the increase in c_y^R intensity can be attributed to the Er^{3+} - Fe^{3+} , Er^{3+} - Dy^{3+} , and Dy^{3+} - Dy^{3+} exchange interactions. Though optical spectroscopy studies on DyFeO_3 and DyAlO_3 suggest only a stronger dipole interaction which leads to the g_x^R -type ordering of Dy^{3+} moments below 4 K, our first principles calculations suggest a strong exchange interaction can also exist between the Dy^{3+} moments. Additionally, the Er^{3+} - Dy^{3+} exchange interactions which are higher than the Dy^{3+} - Dy^{3+} interactions also facilitate the polarization of $\text{Er}^{3+}/\text{Dy}^{3+}$ moments in the c_y^R arrangement.

Below 4 K, due to sudden development of a magnetic peak related to the c_z^R -type arrangement, the total R^{3+} sublattice magnetic moment shows a sudden increase. Similar behavior is observed in ErFeO_3 , in which below 5 K the Er^{3+} moments order as c_z^R along with an increase in ΔE , which attains a maximum value of 6.5 cm^{-1} (0.8 meV or 10 K) [78]. In orthochromate ErCrO_3 , a discontinuity in ΔE occurs at T_{SR} [80] accompanied by the c_z^R ordering of Er^{3+} moments. Usually, in orthoferrites, R^{3+} - R^{3+} and R^{3+} - Fe^{3+} exchange interactions, in comparison to the dipolar interactions, are considered important for determination of the magnetic ground state of the rare-earth moments. But, due to the large magnetic moment of the Er^{3+} and Dy^{3+} moments and the highly localized nature of the $4f$ electrons of $\text{Er}^{3+}/\text{Dy}^{3+}$, the role of magnetic dipolar interactions cannot be neglected, and it may exceed the negligible R^{3+} - R^{3+} exchange interactions, particularly in the case

of Er^{3+} . This is also clear from various optical spectroscopy measurements performed to examine the Kramer’s doublet in various Er^{3+} - and Dy^{3+} -based oxides [52,54,78–81,91]. The Er^{3+} - Er^{3+} dipole interaction which causes the c_z^R ordering is maximum between Er^{3+} moments along the c direction [80,81].

Even though the dipole interactions result in magnetic ordering of the R^{3+} ions at the lowest temperature, the direction of the moments is decided by the anisotropic \mathbf{g} tensor. From optical spectra of ErFeO_3 , it was observed that $g_{xx}(\text{min}) = 1.2$, $g_{yy}(\text{max}) = 4.5$ and g_{zz} ($z||c$ axis) = 5.6 in a - b plane [81]. Thus, a slightly larger anisotropy along the z axis facilitates the c_z^R ordering of the Er^{3+} moments below 5 K. In Dy^{3+} , $g_{xy}(\text{min}) = 3.2$, $g_{xy}(\text{max}) = 18.4$, $g_{zz} = 2.0$, due to which the Dy^{3+} moments have a strong Ising character with moments in the direction of $g_{xy}(\text{max})$ [52], which is also clear from the long-range antiferromagnetic ordering of Dy^{3+} moments with the $\Gamma_5(g_x^R, a_y^R)$ configuration in DyFeO_3 , DyAlO_3 , and DyScO_3 . Thus the c_z^R is completely opposed by the a - b plane anisotropy, even though optical studies on DyAlO_3 reveal that Dy^{3+} - Dy^{3+} dipole interaction has maximum strength along the c direction [91]. Estimate of the dipolar energy in DyScO_3 for various magnetic configurations in the a - b plane reveal that for the experimental (g_x^R, a_y^R) configuration, the lowest dipolar energy (-3.61 K) is achieved, which is also close to the T_{N2} , while the (f_x^R, c_y^R) has the highest energy ($+2.44$ K) at zero field [54].

In a similar manner, an estimate of the ground-state energy of the rare earth in the context of dipolar energy is carried out in EDFO. The magnitude of magnetic moments is fixed according to the experimentally obtained values. The dipolar energy is calculated for Er and Dy arranged alternately for a radii of nearly 6 Å containing 18 atoms. For the four magnetic arrangements, $c_z^R, c_y^R, (c_x^R, c_z^R)$ and (g_x^R, a_y^R), the energies obtained are $-0.158, +0.092, -0.08$, and -0.138 K, respectively. Thus the c_z^R -type polarization is most favored by the Er^{3+} - Dy^{3+} dipolar interaction, while the c_y^R one is least favored. However, the character of the \mathbf{g} tensor of Dy^{3+} tends to suppress the c_z^R polarization to a lower temperature, due to which the peaks appear only at 2 K with a lower magnetic moment than observed in ErFeO_3 .

D. Symmetry of the ground state

Finally, we discuss the symmetry aspects of the magnetic structure of EDFO at 1.5 K. Based on the representation analysis, the resultant magnetic structure can be written as $\Gamma_4 + \Gamma_2 + \Gamma_1$ wherein Γ_1 corresponds to the magnetic structure of the $\text{Er}^{3+}/\text{Dy}^{3+}$ and Fe^{3+} (possibly) sublattices, Γ_2 corresponds to the combined magnetic structure of Fe^{3+} and $\text{Er}^{3+}/\text{Dy}^{3+}$ sublattices, while Γ_4 corresponds to the Fe^{3+} sublattice. To simplify things, we consider the net magnetic structure at 1.5 K as combinations of Γ_{24}, Γ_{14} , and Γ_{12} . The Γ_{12} and Γ_{14} belong to the point group $C_{2h}(C_{2h})(m)$, while the Γ_{24} belongs to the point group $C_{2h}(C_i)(m')$ [48]. The Γ_{14} and Γ_{12} are invariant under the symmetry operations ($E, \tilde{C}_{2x}, i, i\tilde{C}_{2x}$) and ($E, \tilde{C}_{2z}, i, i\tilde{C}_{2z}$), respectively. On the other hand, the Γ_{24} is invariant under ($E, i, R\tilde{C}_{2y}, iR\tilde{C}_{2y}$). Here i corresponds to the inversion symmetry operation and R corresponds to

the time-reversal symmetry operator. In the case of Γ_{24} , there occurs an effective field, which is absent in the case of Γ_1 . Considering the coexistence of three phases, the only symmetry elements remaining are (E, i) . The presence of inversion symmetry rules out the possibility of a spontaneous ferroelectric polarization. Moreover, reduction in the structural symmetry due to the simultaneous presence of c_y^R and c_z^R does not occur, unlike as speculated by Deng *et al.* [8]. The absence of any ferroelectric polarization or magnetodielectric effect is also confirmed by temperature-dependent dielectric studies in the presence of the magnetic field (data not shown).

However, the coexistence of c_y^R and c_z^R structures coincides with a negative volume expansion occurring below 10 K as shown in Fig. 2(e). Though this suggests a magneto-volume effect, the detailed analyses are beyond the scope of this paper.

VI. CONCLUSION

In conclusion, we have investigated magnetic behavior of polycrystalline EDFO using various experimental techniques like bulk magnetization, neutron powder diffraction, and specific heat, while the observed properties were correlated with theoretical estimations from density functional theory. At 300 K, the magnetic structure belongs to the Γ_4 configuration. The 50% substitution of Er^{3+} and Dy^{3+} results in a complex spin reorientation of EDFO. The gradual $\Gamma_4 \rightarrow \Gamma_2$ reorientation of the Fe^{3+} spins begins below 75 K. However, the reorientation remains incomplete even at 10 K, and the magnetic structure with two representation continues to coexist at lower temperatures. The ordering of rare earth due to

its polarization starts below 10 K resulting in a c_y^R peak in the Γ_2 representation. At 2 K, the sudden development of the peak related to a c_z^R -type magnetic structure occurs, though a clear confirmation of G_y -type magnetic structure (having Γ_1 representation) of Fe^{3+} spins is not obtained from the analysis of the neutron diffraction data. The specific heat shows a Schottky peak of relatively larger intensity, indicating the absence of a second-order phase transition. The strengths of exchange interactions estimated from density functional theory calculations suggest that the Er^{3+} - Fe^{3+} , Er^{3+} - Dy^{3+} , and Dy^{3+} - Dy^{3+} exchange interactions are of comparable strength, while the Er^{3+} - Er^{3+} and Dy^{3+} - Fe^{3+} interactions are the weakest. The c_y^R -type magnetic structure of rare-earth magnetic moments is consistent with experimental data. The development of c_z^R can be attributed to the Er^{3+} - Er^{3+} dipole interactions, while the strong anisotropy of Dy^{3+} ions tends to suppress this transition to lower temperature.

ACKNOWLEDGMENTS

This work was supported by the UGC-DAE Consortium for Scientific Research (CSR) and Science and Engineering Research Board (SERB) through CRS-M-228 and CRG/2021/006408, respectively. We acknowledge the support from IIT Roorkee through a SMILE-13 grant. A.S. and S.R. acknowledge MHRD for research fellowships. C.M.N.K. and W.T. acknowledge support from the Narodowa Agencja Wymiany Akademickiej (NAWA) under the Polish Returns 2019 program, Grant No. PPN/PPO/2019/1/00014.

-
- [1] J. Guo, L. Cheng, Z. Ren, W. Zhang, X. Lin, Z. Jin, S. Cao, Z. Sheng, and G. Ma, *J. Phys.: Condens. Matter* **32**, 185401 (2020).
- [2] R. V. Mikhaylovskiy, T. J. Huisman, A. I. Popov, A. K. Zvezdin, T. Rasing, R. V. Pisarev, and A. V. Kimel, *Phys. Rev. B* **92**, 094437 (2015).
- [3] R. V. Mikhaylovskiy, E. Hendry, A. Secchi, J. H. Mentink, M. Eckstein, A. Wu, R. V. Pisarev, V. V. Kruglyak, M. I. Katsnelson, T. Rasing, and A. V. Kimel, *Nat. Commun.* **6**, 8190 (2015).
- [4] R. V. Mikhaylovskiy, E. Hendry, V. V. Kruglyak, R. V. Pisarev, T. Rasing, and A. V. Kimel, *Phys. Rev. B* **90**, 184405 (2014).
- [5] K. Yamaguchi, T. Kurihara, Y. Minami, M. Nakajima, and T. Suemoto, *Phys. Rev. Lett.* **110**, 137204 (2013).
- [6] S. Ding, M. Xue, Z. Liang, Z. Liu, R. Li, S. Cao, Y. Sun, J. Zhao, W. Yang, and J. Yang, *J. Phys.: Condens. Matter* **31**, 435801 (2019).
- [7] A. V. Kimel, A. Kirilyuk, A. Tsvetkov, R. V. Pisarev, and T. Rasing, *Nature (London)* **429**, 850 (2004).
- [8] G. Deng, P. Guo, W. Ren, S. Cao, H. E. Maynard-Casely, M. Avdeev, and G. J. McIntyre, *J. Appl. Phys.* **117**, 164105 (2015).
- [9] Y. Du, Z. X. Cheng, X. L. Wang, and S. X. Dou, *J. Appl. Phys.* **107**, 09D908 (2010).
- [10] Y. Tokunaga, S. Iguchi, T. Arima, and Y. Tokura, *Phys. Rev. Lett.* **101**, 097205 (2008).
- [11] H. Yokota, T. Nozue, S. Nakamura, H. Hojo, M. Fukunaga, P.-E. Janolin, J.-M. Kiat, and A. Fuwa, *Phys. Rev. B* **92**, 054101 (2015).
- [12] A. Singh, S. Rajput, B. Padmanabhan, K. Kedarsh, M. Anas, T. Maitra, and V. K. Malik, *J. Phys.: Condens. Matter* **31**, 355802 (2019).
- [13] Y. J. Ke, X. Q. Zhang, Y. Ma, and Z. H. Cheng, *Sci. Rep.* **6**, 19775 (2016).
- [14] T. Chakraborty, R. Yadav, S. Elizabeth, and H. L. Bhat, *Phys. Chem. Chem. Phys.* **18**, 5316 (2016).
- [15] K. Knižek, J. Hejtmánek, Z. Jirák, P. Tomeš, P. Henry, and G. Andre, *Phys. Rev. B* **79**, 134103 (2009).
- [16] W. Sławiński, R. Przeniosło, I. Sosnowska, and E. Suard, *J. Phys.: Condens. Matter* **17**, 4605 (2005).
- [17] N. L. Ross, J. Zhao, J. B. Burt, and T. D. Chaplin, *J. Phys.: Condens. Matter* **16**, 5721 (2004).
- [18] A. M. Glazer, *Acta Cryst. B* **28**, 3384 (1972).
- [19] P. M. Woodward, *Acta Cryst. B* **53**, 32 (1997).
- [20] P. M. Woodward, *Acta Cryst. B* **53**, 44 (1997).
- [21] M. Marezio, J. P. Remeika, and P. D. Dernier, *Acta Cryst. B* **26**, 2008 (1970).
- [22] W. C. Koehler, E. O. Wollan, and M. K. Wilkinson, *Phys. Rev.* **118**, 58 (1960).
- [23] R. L. White, *J. Appl. Phys.* **40**, 1061 (1969).
- [24] E. F. Bertaut, in *MAGNETISM: A Treatise on Modern Theory and Materials*, edited by G. T. Rado and H. Suhl (Academic Press, New York, 1963), Vol. III, pp. 149–209.
- [25] T. Yamaguchi, *J. Phys. Chem. Solids* **35**, 479 (1974).
- [26] J. Bartolomé, E. Palacios, M. D. Kuz'min, F. Bartolomé, I. Sosnowska, R. Przeniosło, R. Sonntag, and M. M. Lukina, *Phys. Rev. B* **55**, 11432 (1997).

- [27] H. Horner and C. M. Varma, *Phys. Rev. Lett.* **20**, 845 (1968).
- [28] H. Pinto and H. Shaked, *Solid State Commun.* **10**, 663 (1972).
- [29] I. Sosnowsk, E. Steichelea, and A. Hewatc, *Physica B+C* **136**, 394 (1986).
- [30] R. Przeniosło, I. Sosnowska, P. Fischer, W. Marti, F. Bartolomé, J. Bartolomé, E. Palacios, and R. Sonntag, *J. Magn. Magn. Mater.* **160**, 370 (1996).
- [31] S. Yuan, Y. Wang, M. Shao, F. Chang, B. Kang, Y. Isikawa, and S. Cao, *J. Appl. Phys.* **109**, 07E141 (2011).
- [32] G. Song, J. Jiang, B. Kang, J. Zhang, Z. Cheng, G. Ma, and S. Cao, *Solid State Commun.* **211**, 47 (2015).
- [33] J. Jiang, G. Song, D. Wang, Z. Jin, Z. Tian, X. Lin, J. Han, G. Ma, S. Cao, and Z. Cheng, *J. Phys.: Condens. Matter* **28**, 116002 (2016).
- [34] L. Chen, T. Li, S. Cao, S. Yuan, F. Hong, and J. Zhang, *J. Appl. Phys.* **111**, 103905 (2012).
- [35] R. Przeniosło, I. Sosnowska, and P. Fischer, *J. Magn. Magn. Mater.* **140–144**, 2153 (1995).
- [36] F. Bartolomé, M. D. Kuz'min, J. Bartolomé, J. Blasco, J. García, and F. Sapiña, *Solid State Commun.* **91**, 177 (1994).
- [37] R. M. Bozorth, V. Kramer, and J. P. Remeika, *Phys. Rev. Lett.* **1**, 3 (1958).
- [38] R. W. Grant and S. Geller, *Solid State Commun.* **7**, 1291 (1969).
- [39] Y. B. Bazaliy, L. T. Tsymba, G. N. Kakazei, A. I. Izotov, and P. E. Wigen, *Phys. Rev. B* **69**, 104429 (2004).
- [40] H. Pinto, G. Shachar, H. Shaked, and S. Shtrikman, *Phys. Rev. B* **3**, 3861 (1971).
- [41] L. T. Tsymbal, Y. B. Bazaliy, V. N. Derkachenko, V. I. Kamenev, G. N. Kakazei, F. J. Palomares, and P. E. Wigen, *J. Appl. Phys.* **101**, 123919 (2007).
- [42] G. Gorodetsky, R. M. Hornreich, I. Yaeger, H. Pinto, G. Shachar, and H. Shaked, *Phys. Rev. B* **8**, 3398 (1973).
- [43] G. Gorodetsky, B. Sharon, and S. Shtrikman, *J. Appl. Phys.* **39**, 1371 (1968).
- [44] L. A. Prelorendjo, C. E. Johnson, M. F. Thomas, and B. M. Wanklyn, *J. Phys. C* **13**, 2567 (1980).
- [45] Z. Y. Zhao, X. Zhao, H. D. Zhou, F. B. Zhang, Q. J. Li, C. Fan, X. F. Sun, and X. G. Li, *Phys. Rev. B* **89**, 224405 (2014).
- [46] J. Wang, J. Liu, J. Sheng, W. Luo, F. Ye, Z. Zhao, X. Sun, S. A. Danilkin, G. Deng, and W. Bao, *Phys. Rev. B* **93**, 140403(R) (2016).
- [47] F. J. Morin, *Phys. Rev.* **78**, 819 (1950).
- [48] T. Yamaguchi and K. Tsushima, *Phys. Rev. B* **8**, 5187 (1973).
- [49] A. Berton and B. Sharon, *J. Appl. Phys.* **39**, 1367 (1968).
- [50] I. Nowik and H. Williams, *Phys. Lett.* **20**, 154 (1966).
- [51] K. P. Belov, A. M. Kadomtseva, L. M. Ledneva, T. L. Ovchinnikova, Ya. G. Ponomarev, and V. A. Timofeeva, *Soviet Phys.-Solid State* **9**, 2193 (1968).
- [52] L. M. Holmes, L. G. V. Uitert, R. R. Hecker, and G. W. Hull, *Phys. Rev. B* **5**, 138 (1972).
- [53] I. B. Krynetskii and V. M. Matveev, *Phys. Solid State* **39**, 584 (1997).
- [54] L. S. Wu, S. E. Nikitin, M. Frontzek, A. I. Kolesnikov, G. Ehlers, M. D. Lumsden, K. A. Shaykhtudinov, E. J. Guo, A. T. Savici, Z. Gai, A. S. Sefat, and A. Podlesnyak, *Phys. Rev. B* **96**, 144407 (2017).
- [55] A. K. Zvezdin and A. A. Mukhin, *JETP Lett.* **88**, 505 (2008).
- [56] B. Rajeswaran, D. Sanyal, C. Mahuya, Y. Sundarayya, A. Sundaresan, and C. N. R. Rao, *Europhys. Lett.* **101**, 17001 (2013).
- [57] G. R. Hoogeboom, T. Kuschel, G. E. W. Bauer, M. V. Mostovoy, A. V. Kimel, and B. J. van Wees, *Phys. Rev. B* **103**, 134406 (2021).
- [58] A. Singh, A. Jain, A. Ray, P. B., R. Yadav, V. Nassif, S. Husain, S. M. Yusuf, T. Maitra, and V. K. Malik, *Phys. Rev. B* **96**, 144420 (2017).
- [59] Y. Tokunaga, Y. Taguchi, T. Arima, and Y. Tokura, *Phys. Rev. Lett.* **112**, 037203 (2014).
- [60] M. Mihalik, M. Mihalik, M. Fitta, M. Bałanda, M. Vavra, S. Gabáni, M. Zentková, and J. Briančin, *J. Magn. Magn. Mater.* **345**, 125 (2013).
- [61] T. Chakraborty and S. Elizabeth, *J. Magn. Magn. Mater.* **462**, 78 (2018).
- [62] H. Wu, S. Cao, M. Liu, Y. Cao, B. Kang, J. Zhang, and W. Ren, *Phys. Rev. B* **90**, 144415 (2014).
- [63] J. Lazurova, M. Mihalik, M. Mihalik Jr., M. Vavra, M. Zentkova, J. Briancin, M. Perovic, V. Kusigerski, O. Schneeweiss, P. Roupčova *et al.*, *J. Phys. Conf. Ser.* **592**, 012117 (2015).
- [64] H. S. Nair, T. Chatterji, C. M. N. Kumar, T. Hansen, H. Nhalil, S. Elizabeth, and A. M. Strydom, *J. Appl. Phys.* **119**, 053901 (2016).
- [65] H. Rietveld, *J. Appl. Crystallogr.* **2**, 65 (1969).
- [66] J. Rodriguez-Carvajal, *Physica B (Amsterdam)* **192**, 55 (1993).
- [67] E. Hovestreydt, M. Aroyo, S. Sattler, and H. Wondratschek, *J. Appl. Cryst.* **25**, 544 (1992).
- [68] G. Kresse and J. Furthmüller, *Phys. Rev. B* **54**, 11169 (1996).
- [69] J. P. Perdew, K. Burke, and M. Ernzerhof, *Phys. Rev. Lett.* **77**, 3865 (1996).
- [70] V. I. Anisimov, I. V. Solovyev, M. A. Korotin, M. T. Czyzyk, and G. A. Sawatzky, *Phys. Rev. B* **48**, 16929 (1993).
- [71] C. M. N. Kumar, Y. Xiao, P. Lunkenheimer, A. Loidl, and M. Ohl, *Phys. Rev. B* **91**, 235149 (2015).
- [72] H. Shen, Z. Cheng, F. Hong, X. Jiayue, S. Yuan, S. Cao, and X. Wang, *Appl. Phys. Lett.* **103**, 192404 (2013).
- [73] X. X. Zhang, Z. C. Xia, Y. J. Ke, X. Q. Zhang, Z. H. Cheng, Z. W. Ouyang, J. F. Wang, S. Huang, F. Yang, Y. J. Song *et al.*, *Phys. Rev. B* **100**, 054418 (2019).
- [74] A. Epstein and H. Shaked, *Phys. Lett. A* **29**, 659 (1969).
- [75] A. Singh, S. Rajput, P. Balasubramanian, M. Anas, F. Damay, C. M. N. Kumar, G. Eguchi, A. Jain, S. M. Yusuf, T. Maitra, and V. K. Malik, *Phys. Rev. B* **102**, 144432 (2020).
- [76] E. F. Bertaut, *Acta Cryst.* **A24**, 217 (1968).
- [77] K. Saito, Y. Yamamura, J. Mayerb, H. Kobayashi, Y. Miyazakia, J. Ensling, P. Gütlich, B. Leśniewska, and M. Sorai, *J. Magn. Magn. Mater.* **225**, 381 (2001).
- [78] R. Faulhaber, S. Hübner, E. Orlich, and H. Schuchert, *Z. Phys.* **204**, 101 (1967).
- [79] H. Schuchert, S. Hübner, and R. Faulhaber, *Z. Phys.* **220**, 273 (1969).
- [80] A. Hasson, R. M. Hornreich, Y. Komett, B. M. Wanklyn, and I. Yaeger, *Phys. Rev. B* **12**, 5051 (1975).
- [81] D. L. Wood, L. M. Holmes, and J. P. Remeika, *Phys. Rev.* **185**, 689 (1969).
- [82] S. L. Dudarev, G. A. Botton, S. Y. Savrasov, C. J. Humphreys, and A. P. Sutton, *Phys. Rev. B* **57**, 1505 (1998).
- [83] C. Weingart, N. Spaldin, and E. Bousquet, *Phys. Rev. B* **86**, 094413 (2012).
- [84] A. K. Zvezdin and V. M. Matveev, *Zh. Exsp. Teor. Fiz.* **77**, 1076 (1979).

- [85] P. Pataud and J. Sivardi re, *J. Phys. France* **31**, 1017 (1970).
- [86] J. D. Cashion, A. H. Cooke, D. M. Martin, and M. R. Wells, *J. Phys. C* **3**, 1612 (1970).
- [87] G. W. Durbin, C. E. Johnson, and M. F. Thomas, *J. Phys. C* **10**, 1975 (1977).
- [88] T. Sakata and A. Enomura, *Phys. Stat. Sol. (a)* **52**, 311 (1979).
- [89] J. Chen, X. Wu, and A. Selloni, *Phys. Rev. B* **83**, 245204 (2011).
- [90] R. M. Horneich, Y. Komet, R. Nolan, B. M. Wanklyn, and I. Yaeger, *Phys. Rev. B* **12**, 5094 (1975).
- [91] H. Schuchert, S. H ufner, and R. Faulhaber, *Z. Phys.* **222**, 105 (1969).